AKADÉMIAI KIADÓ

UNIVERSITY of DEBRECEN

International Review of Applied Sciences and Engineering

14 (2023) 2, 183–200

DOI:
10.1556/1848.2022.00474

ORIGINAL RESEARCH PAPER

Hybrid MDA-ANFIS approach based control of grid connected solar system with nine level inverter wind energy conversion

A. Apparao[1,2*] and G. Chandra Sekhar[3]

[1] NEFT University, Aalo, India

[2] Department of Electrical and Electronics Engineering, SVCET, Etcherla, Srikakulam, Andhra Pradesh, India

[3] Department of Electrical and Electronics Engineering, GMR Institute of Technology, Rajam, Andhra Pradesh, India

Received: February 2, 2022 • Accepted: June 1, 2022
Published online: February 14, 2023

ABSTRACT

A hybrid approach is proposed in this paper to achieve the load power requirement for grid connected hybrid photovoltaic wind system. The proposed approach is the combined execution of both the Modified Dragonfly Algorithm (MDA) and Adaptive Neuro-Fuzzy Interference System (ANFIS), hence it is called MDA-ANFIS. ANFIS approach is improved by the MDA approach to minimize the error functions. The main aim of the proposed approach is satisfying the load power requirement and obtains the maximum energy from the hybrid wind solar system. Through the modelling of operating modes of generation units, the proposed approach determines the switching states of the inverter. The MDA approach is utilized to generate the dataset and the data set is processed by ANFIS, which creates the control signal. By using the proposed approach, it was possible to minimize the system parameter radiation, external disturbances as well as optimally fulfill the load demand. The proposed method is activated in MATLAB/Simulink platform, and its performance is compared with existing methods.

KEYWORDS

hybrid PV wind system, error functions, maximum energy, modified dragonfly algorithm, adaptive neuro-fuzzy interference system

1. INTRODUCTION

In the current years, the Hybrid Renewable Energy Sources (HRES) is growing rapidly which has guaranteed to satisfy increasing energy requirement [1]. The reason for its success is being appropriate and the nature of nonpolluting [2]. The power supply reliability is increased by the concurrent use of hybrid system as well as more number of RES [3]. The hybrid wind and solar is popular among these various RES which is also in the organized manner [4]. One of the wonderful resources is wind power because it is obtained in an easy way and by the wind turbines it is gathered with high power capacitance [5]. Another guaranteed green energy source is the solar energy, which is simply obtained by using photovoltaic modules [6–10].

Actually, owing to night and cloudy days, the power of solar is very low; at that time strong winds occur mainly with wind and solar power potential [11]. At the same time, weak winds usually occur during the summer [12]. Hence, through the unstable environmental circumstances, the introduction of hybrid wind-solar energy conversion system offers unique power production with permanent output power [13]. The utilization of hybrid solar and wind system connected with grid is increased considerably by the sudden development of

*Corresponding author.
E-mail: apparaoanem@gmail.com

AKJournals

power electronic devices and the organization approaches [14]. To achieve the effective power conversion based on HRES, the rectifier, boost converters and inverters play an important role [15]. For each power generation system, the individual or combined DC/DC converter can be used [16]. Moreover, another essential configuration is DC/AC converter configuration and its control mechanism [17].

Presently, multi-level inverter (MLI) topologies are highly preferred as they have extra advantages [18]. MLI has ability to manage the high voltages together with the characteristics, like good noise minimization, excellent electromagnetic compatibility, low pressure voltage in switches [19]. In the RES, grid integration ideal characteristics, like many conventional symmetric, asymmetric and device number control algorithms, modulation methods with multi-level inverter topologies are utilized [20]. In the operation of hybrid wind solar system, the voltage variations, harmonic production, flickering, unbalanced dc connection capacitor voltage producing affect the quality of power [21]. Because of the power converter, some unnecessary harmonics are produced. The output power for solar and wind system depends on the solar ultraviolet radiation together with speed of wind [22]. Based on variable wind speed, power generation/voltage difference occurs in the output power. Based on the variation of DC connection capacitor voltages, a maximum DC current in the DC capacitor connection is varied [23]. Therefore, MLI topologies are connected to control the DC connection voltage in the grid integrated system [24].

In this paper, a hybrid approach is proposed to achieve the load power requirement for grid connected hybrid photovoltaic wind system. The proposed hybrid approach is the combination of MDA and ANFIS called MDA-ANFIS. To minimize the error functions, ANFIS approach is improved by the MDA approach. The major aim of the proposed method is fulfilling the load power requirement and obtaining the maximum energy from the hybrid wind solar system. The rest of this paper is organized as follows: Section 2 describes the recent studies. Section 3 illustrates the 3 phase hybrid wind-photovoltaic network with nine-level inverter. Section 4 depicts the control method for the nine-level inverter that is dependent on grid-connected wind, PV system utilizing proposed approach. Section 5 explains about the proposed approach with grid connected system. Section 6 provides the result and discussion. Section 7 concludes the paper.

2. RECENT RESEARCH WORKS: A BRIEF REVIEW

Several studies were previously presented in the literature based on power electronics with HRES utilizing certain methods and features. Some of the recent works are reviewed here.

Asano et al., [25] have suggested three-level inverter with combined power sources and energy storage device for raising the regenerative power. The regenerated energy was utilized by a charge and discharge control process. By the use of scaled-down model and numerical simulation the introduced approach performance was evaluated. Das et al., [26] have suggested the unbalanced multi-level inverter for PV system. The suggested approach used the minimum number of switches. The DC voltage was achieved by the connection of PV module of unbalanced power rating to the asymmetric layer multi-level inverter in a proper manner. PV power, voltages and phase current were controlled to attain maximal power with sinusoidal current by a single power point, using separate maximum power point tracking, voltage monitors, current controlled approaches. V. Pires et al., [27] have presented the multilevel 3 phase voltage source inverter (VSI) for the PV system. The presented phase 2 level voltage source inverter, isolation transformer. The DC side of every 3 phase voltage source inverter was attached to the photovoltaic panels. To guarantee the various stages, the ac side of every 3 phase voltage source inverter was attached to the open end winding of the three-phase isolation transformer. The VSI was modulated by the PWM approach. Mahendiran [28] has developed a hybrid approach with cascaded multilevel inverter for a grid connected hybrid system. The hybrid approach was the combined operations of color harmony algorithm and extreme gradient boosting called CHA-XGBOOST. Gain parameter of the proposed controller was generated by the design of CMLI. The aim was to achieve the power demand and obtains the maximum power of the solar wind system. Evaluation of gain parameters were obtained by the CHA in offline way and control parameters were obtained by XGBOOST by online.

Saravanan and Sivakumaran [29] have introduced an IDE-GBDT approach including multiple output converter and multiple level inverter for solar PV system. The introduced method was the combination of dolphin echolocation process and gradient boosting decision trees. The introduced approach was utilised the modified incremental conductance method for acquiring maximal power of the photovoltaic system. For producing various balanced result, the multi-output converter was incorporated with the boost converter along a switched capacitor. The introduced approach reduced the loss and the improved the efficiency of the PV system. Sharma et al., [30] have suggested cascaded H-Bridge multilevel inverter (CHBMLI) depending on the grid connected hybrid RES system. Through the dc link of the CHBMLI, the wind and solar system was incorporated individually. The PWM rectifier was utilised for reducing the harmonics of the system. An unbalanced voltage of the suggested approach was balanced by the isolated dc-links. Ali et al., [31] have presented the dc-ac Cascaded Transformer base Modular Multilevel Inverter (CTMLI) using PWM approach for PV application. The presented approach was switching the input dc voltage to nineteen-level ac voltage by three full-bridge (FB) circuits. The presented approach was used the transformer turn's ratio and cost estimation model for minimizing the price of the CTMLI.

2.1. Background of the research work

The review of recent studies shows that the optimal control of grid-connected hybrid generation scheme with the help of solar, wind energy is a noteworthy contributing factor. Nevertheless, at grid-connected hybrid photovoltaic-wind utilizations, the variations of load requirement and meteorological data viz, irradiation, temperature, wind speed are the primary issues. These disruptions often occur owing to the complex control of various energy sources. Several approaches are activated to control the hybrid renewable energy production; they are active power control (APC) along with anti-windup proportional integral (AWPI) controller, fuzzy logic control, Genetic algorithm, Particle Swarm Optimization, etc. Here, the APC and AWPI both do not deem overall production cost, moreover, they do not fit the micro grid complexity. Fuzzy logic controller needs a number of data. It is no more feasible for programs lesser or greater than historical data. The major disadvantages of Genetic algorithm and Particle Swarm Optimization are their very sluggish processing as well as their inability to recognize the optimal solution. A few control approaches were suggested in the literature for optimally controlling the grid-connected hybrid power generation, but the suggested approaches are ineffective. These shortcomings have caused to do this work to be carried out.

3. GRID CONNECTED HYBRID PV WIND SYSTEM WITH NINE-LEVEL INVERTER

The overall structure of the proposed approach is presented in Fig. 1.

Then the grid connected hybrid system consists of PV, wind, grid, nine-level inverter, PWM. The wind and solar system are connected to the dc bus of the system. The solar method is the process of generating the dc energy related to the natural radiation, temperature. It consists of dc-dc converter, PV panel. When electricity is generated via the wind it is known as the wind system. Wind energy system is incorporated with permanent magnet synchronous generator (PMSG), ac to dc converter and dc to dc converter. A source of output power is given to the nine-level inverter which processes the input by the use of the proposed MDA-ANFIS approach. The PWM is used to produce the control signal that is given to the nine-level inverter.

3.1. Modelling of wind generating units

The wind power is generally produced by the stochastic wind speed of environment. In general, the stochastic wind speed probability density function is exhibited as,

$$p_v(v) = \frac{s_i}{c}\left(\frac{v}{c}\right)\exp\left[-\left(\frac{v}{c}\right)^k\right] \tag{1}$$

where Weibull distribution shape index and scale index is indicated as k and c. The output power of the wind is described as

$$P_{wind} = \begin{cases} 0, & v<v_{in} \\ P_n\left(b_1v^3 + b_2v^2 + b_3v + b_4\right), & v_{in} \le v<v_N \\ P_n, & v_n \le v<v_{out} \\ 0, & v \ge v_{out} \end{cases} \tag{2}$$

here fitting coefficients is denoted as b_1, b_2, b_3, b_4, active power is denoted as P_{wind} and wind production units output power rate is denoted as P_n, wind speed in wind unit hub height, wind speed rated, cut in wind speed and cut out wind speed are denoted as v, v_N, v_{in}, v_{out} respectively.

3.2. Modelling of PV generating units

The output power of PV depends on light intensity, PV area and efficiency. The probability density function is described as,

$$P(i) = \frac{\kappa(\alpha+\beta)}{\kappa(\alpha)\kappa(\beta)}\left(\frac{i_{pv}}{i_{pv}^{\max}}\right)^{\alpha-1}\left(1-\frac{i_{pv}}{i_{pv}^{\max}}\right)^{\beta-1} \tag{3}$$

In this, the shape indexes, such as the beta distribution is denoted as α, β, maximum PV current is specified as $I_{pv}^{\max}$, gamma function is specified as κ. From that the output of PV is determined by,

$$P\left(P_{pv}\right) = \frac{\kappa(\alpha+\beta)}{A.\eta\kappa.(\alpha)\kappa(\beta)}\left(\frac{P_{pv}}{P_{pv}^{\max}}\right)^{\alpha-1}\left(1-\frac{P_{pv}}{P_{pv}^{\max}}\right)^{\beta-1} \tag{4}$$

$$P_{pv} = A.\eta.I_{pv} \tag{5}$$

3.3. DC-DC converter model

The dc bus voltage is obtained by the dc-dc converter. The duty cycle of the converter is expressed as,

$$d_c = 1 - \left(\frac{V_i}{V_o}\right) \tag{6}$$

here input voltage is denoted as V_i, output voltage is denoted as V_o.

3.4. Nine-level inverter model

The nine level inverter consist of more number of switches but it has many advantages, like low voltage stress, high output voltage, low loss, low harmonic distortion. It is used for FACTS devices and many applications. The nine-level inverter is connected to the proposed approach. It produces the sinusoidal voltage and the output consists of $2n+1$ number [32]. Through the adjustment of switching angles, the total harmonic minimization is obtained. It consists of 16 switching control. The 9-level inverter is under the type of H bridge inverter. Each inverter level is producing the different output voltage. The nine-level H-bridge is formed by 4-H-bridge connected in every phase. Each of the H-bridges needs individual DC source. Every phase needs n-bridge which is incorporated in a series manner and it produces the 2n+1 level. For the 9-level inverter consist of 729 switching instants. Among 729 switching moments, independent switching instant are 217 and redundancies

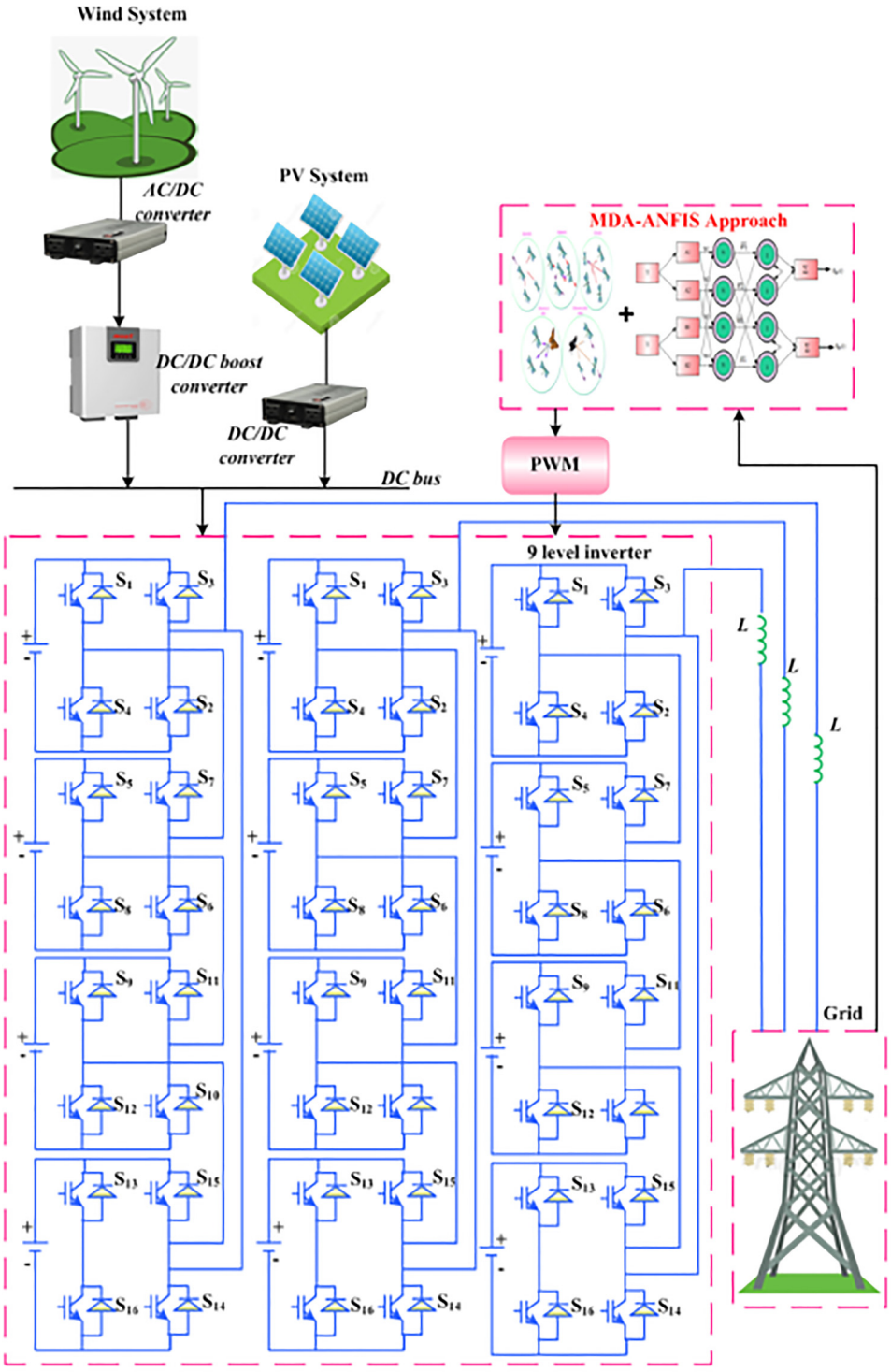

Fig. 1. Over all architecture of the proposed system

switching moment are 512. In the space vector diagram it consists of 8 layer as well as 512 triangles. The output of nine-level inverter is described as,

$$V_o = V_{i1} + V_{i2} + V_{i3} + V_{i4} + V_{i5} + V_{i6} + V_{i7} + V_{i8} + V_{i9} \tag{7}$$

Through the PWM the inverter gets the control signal, so the modulation index is described as,

$$M = \frac{\sqrt{3}v_{re}}{E} \tag{8}$$

The switching states produce different output. It satisfies the following equation,

$$V_{dcn} = \frac{2}{2n+1}\sum_{m=0}^{n} v_m \tag{9}$$

3.5. Voltage and current harmonic distortion

The active on linear devices are present in the system which produces the harmonics. To determine the performance of the system one must determine the total voltage harmonic distortion and total current harmonic distortion. The ratio of sum of the power of all harmonic current apparatus to the power of the fundamental current frequency is called as total current harmonic distortion which is described by,

$$TVHD = \frac{100\times\sqrt{v_{rms}^2 - v_{frms}^2}}{v_{frms}} \tag{10}$$

$$TIHD = \frac{100\times\sqrt{i_{rms}^2 - i_{frms}^2}}{i_{frms}} \tag{11}$$

here *TVHD* denotes total voltage harmonic distortion, *TIHD* denotes total current harmonic distortion, v_{frms} denotes fundamental voltage frequency, i_{frms} denotes fundamental current frequency, v_{rms} denotes harmonic voltage component, i_{rms} denotes harmonic current component.

3.6. Steady state error

The variation between the input and output of a system is described as steady state error, which limit of time is goes to infinity.

$$e(\tau) = \lim_{m\to 0}\frac{mR(m)}{1+G(s)} \tag{12}$$

3.7. Constraints

3.7.1. Power balance. Power balancing is one of the important factors for fulfilling the needs of power demand. If the system power is balanced, then the system safety is provided with minimum cost. It consists of PV, then the wind power balance is equal to the load power, which is described by,

$$P_{pv} + P_{wind} = P_L \tag{13}$$

here the load power is denoted as P_L output power of PV, wind is denoted as P_{pv}, P_{wind} respectively.

3.7.2. Generation capacity. The generation power limit is described as,

$$P^i_{\min} + P^i = P^i_{\max} \tag{14}$$

here minimum and maximum power of RES under *i* th unit is denoted as $P^i_{\min}$, $P^i_{\max}$ respectively.

4. CONTROL METHODOLOGY OF PROPOSED APPROACH

Figure 2 displays the control process of the proposed approach. Initially, three phase input is given to the inverter which is attached to the grid. Here, two processes like current control and voltage control are processed. First, the current signal is transferred to the Clarke's transformation which transforms the signal to the stationary frame. Park's transformation is used to transform the signal to reference frame. The analysis of current and voltage is described as,

$$\begin{bmatrix} I^\alpha \\ I^\beta \end{bmatrix} = \sqrt{\frac{2}{3}}\begin{bmatrix} 1 & \frac{-1}{2} & \frac{-1}{2} \\ 0 & \frac{\sqrt{3}}{2} & \frac{-\sqrt{3}}{2} \end{bmatrix} \times \begin{bmatrix} I_a \\ I_b \\ I_c \end{bmatrix} \tag{15}$$

Frame is transferred to the d q frame then the equation become

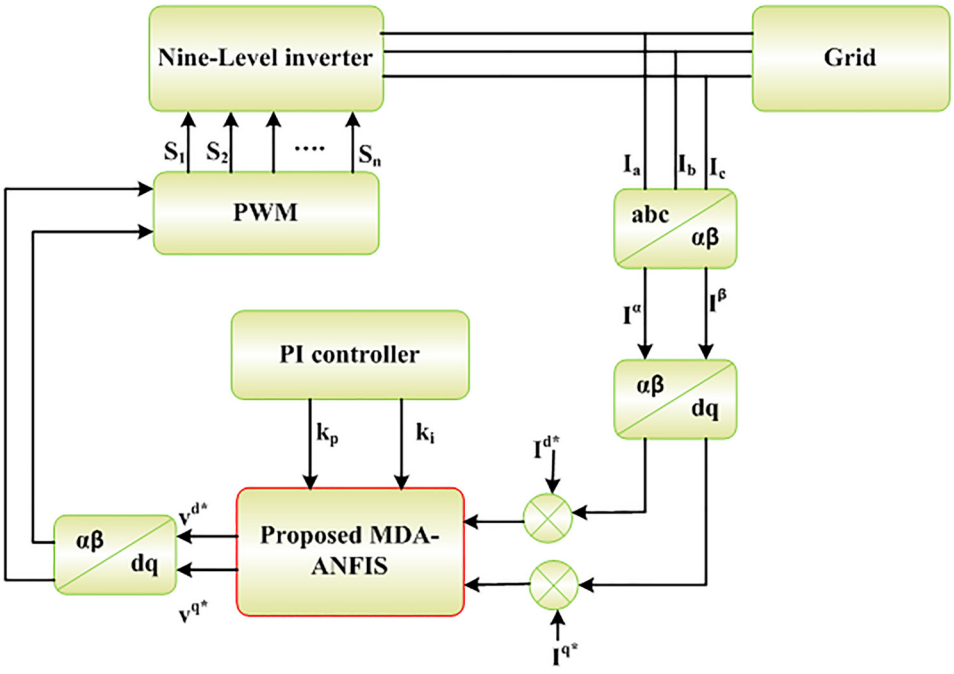

Fig. 2. Control method of proposed approach

$$\begin{bmatrix} I^d \\ I^q \end{bmatrix} = \begin{bmatrix} \sin st & -\cos st \\ \cos st & \sin st \end{bmatrix} \times \begin{bmatrix} I^\alpha \\ I^\beta \end{bmatrix} \tag{16}$$

The dq frame is compared to the error signal from that the error signal is determined by,

$$E = e_1 + e_2 \tag{17}$$

$$e_1 = I^{d*} - i^d \tag{18}$$

$$e_2 = I^{q*} - i^q \tag{19}$$

The PI controller produces the gain parameter which is controls the error signal of the proposed approach. The controller is generate the reference signal which is used to eliminate the error function of the system.

5. PROPOSED MDA-ANFIS APPROACH IN GRID CONNECTED HYBRID PV WIND SYSTEM

In this work, the hybrid MDA-ANFIS approach with nine level inverter is proposed to obtain the load power requirement and maximum power of the system. By the modelling of hybrid PV wind system, the switching states of nine-level inverter are calculated. Combined execution is applied, such as the modified dragonfly algorithm and the adaptive Neuro-Fuzzy Interference System (ANFIS) known as MDA-ANFIS approach. To minimize the error function of the system the MDA approach is used and the optimal output of the MDA is processed by the ANFIS which produce the optimal control signal.

5.1. Data generation using modified dragonfly algorithm (MDA)

The dragonfly process is motivated through the behavior of drone flies. In general, a significant characteristic of the dragon flies are constant and dynamic swarm behaviors of dragon flying. There are two different stages are used in this algorithm that are exploitation and exploration [33]. These two stages are modeled by some behavior, viz interactions of dragon flies, searching for food, avoiding enemies. If the behavior of dragonflies is not predatory swarm behavior, and is known as static swarm behavior, that is characterized by a small group of dragonflies which moves inward, change hierarchies. The separation, alignment, synchronization and distraction of food sources and enemy sources determine the dragonflies' movements. To enhance the dragonfly algorithm, the proposed approach uses the cross over and mutation process. Using this process, the ability of searching is improved. Hence it is called a modified dragonfly algorithm. In the proposed method, the MDA is utilized for generating the data set of system.

5.1.1. Step by step process of MDA.

Step 1: Initialization

Initially, gain parameters are given as input and then it is randomly developed the parameters in the following format,

$$X_i = \begin{bmatrix} {k_p}^{11}{k_i}^{11} & {k_p}^{12}{k_i}^{12} & \cdots & {k_p}^{1n}{k_i}^{1n} \\ {k_p}^{21}{k_i}^{21} & {k_p}^{22}{k_i}^{22} & \cdots & {k_p}^{2n}{k_i}^{2n} \\ \vdots & \vdots & \vdots & \vdots \\ {k_p}^{m1}{k_i}^{m1} & {k_p}^{m2}{k_i}^{m2} & \cdots & {k_p}^{mn}{k_i}^{mn} \end{bmatrix} \tag{20}$$

here k_p and k_i specifies the gain parameters.

Step 2: Fitness Evaluation

The fitness of every dragonfly is subjected to the initial values, and it is calculated below,

$$f = \begin{bmatrix} f_1\ [{k_p}^{11}{k_i}^{11} & {k_p}^{12}{k_i}^{12} & \cdots & {k_p}^{1n}{k_i}^{1n}] \\ f_2\ [{k_p}^{21}{k_i}^{21} & {k_p}^{22}{k_i}^{22} & \cdots & {k_p}^{2n}{k_i}^{2n}] \\ \vdots & \vdots & \vdots & \vdots \\ f_n\ [{k_p}^{m1}{k_i}^{m1} & {k_p}^{m2}{k_i}^{m2} & \cdots & {k_p}^{mn}{k_i}^{mn}] \end{bmatrix} \tag{21}$$

The objective function is specified as,

$$Obj\ F_i = Min\ e \tag{22}$$

At the time, the process can be optimal when the minimum objective function is reached. After the fitness calculation, an estimate of separation, alignment, cohesion coefficients is calculated to update the position and speed of the dragonflies.

Step 3: Separation

Separation indicates the avoidance of persistent conflicts between the individuals of another neighborhood, which is calculated by,

$$S_i = -\sum_{i=1}^{N} d - d_i \tag{23}$$

Step 4: Alignment

Alignment refers to the speed coincidence of individuals with other nearby counts, that is calculated by,

$$A_i = \frac{\sum_{i=1}^{N} v_i}{l} \tag{24}$$

Step 5: Cohesion

This is defined as the distribution of segment and centered, based on the mass neighborhood, and is calculated by,

$$C_i = \frac{\sum_{i=1}^{N} d_i}{N} - d \tag{25}$$

here v_i, d_i indicates the velocity and position of the ith individual. The current individual status d and N denotes the number of neighbours.

Step 6: Attraction and distraction

Gravity in the direction of food source, fly from opponent and distraction are described as,

$$F_i = d^+ - d \tag{26}$$

$$E_i = d^- + d \tag{27}$$

Step 7: Updating

Upgrading procedure of dragonflies is modified by crossover and mutation process, the speed of the dragonfly if there is at least one dragonfly in the neighborhood. Dragonflies' global search capability has been enhanced by this process.

Step 8: Crossover and Mutation

The crossover and the mutation functions are utilized for improving the efficacy of the algorithm. In this, the crossovers are achieved among 2 individuals. During the process of mutation, the individuals are mutated randomly depending on the specified fitness function.

The crossover and mutation are expressed as,

$$Boundary = \frac{\gamma_n}{L_c} \tag{28}$$

$$Evolution = \frac{\lambda_m}{L_c} \tag{29}$$

where γ_n signifies the number of individuals crossover, λ_m signifies the mutation point and L_c represents the length of prey.- Finding the fitness and checking the objective function uses the updated movement. If the above mentioned steps are completed once, then it is possible to select the optimal dataset.

5.2. Optimal control signal prediction using ANFIS approach

Adaptive Neuro-Fuzzy Interference System is the artificial neural network category that depends on the Takagi- Sugeno fuzzy inference system. It consists of neural networks in a fuzzy system. There are five layers present in the ANFIS process in which the layers consist of nodes [34]. The ANFIS five layers are fuzzification process, past piece of fuzzy rules, membership of normalization functions, fuzzy rules of the consequent piece, output of network. Sugeno hybrid training algorithm is utilized to determine the parameters of the fuzzy system. The optimal control signals are predicted utilizing ANFIS. Figure 3 shows the flowchart of the proposed MDA-ANFIS approach. The process of each layer is described as below.

5.2.1. Step by step process of ANFIS. *1st Layer:* In the first layer ANFIS is weighted by some weight factors like W_{yz}^3, W_y^2

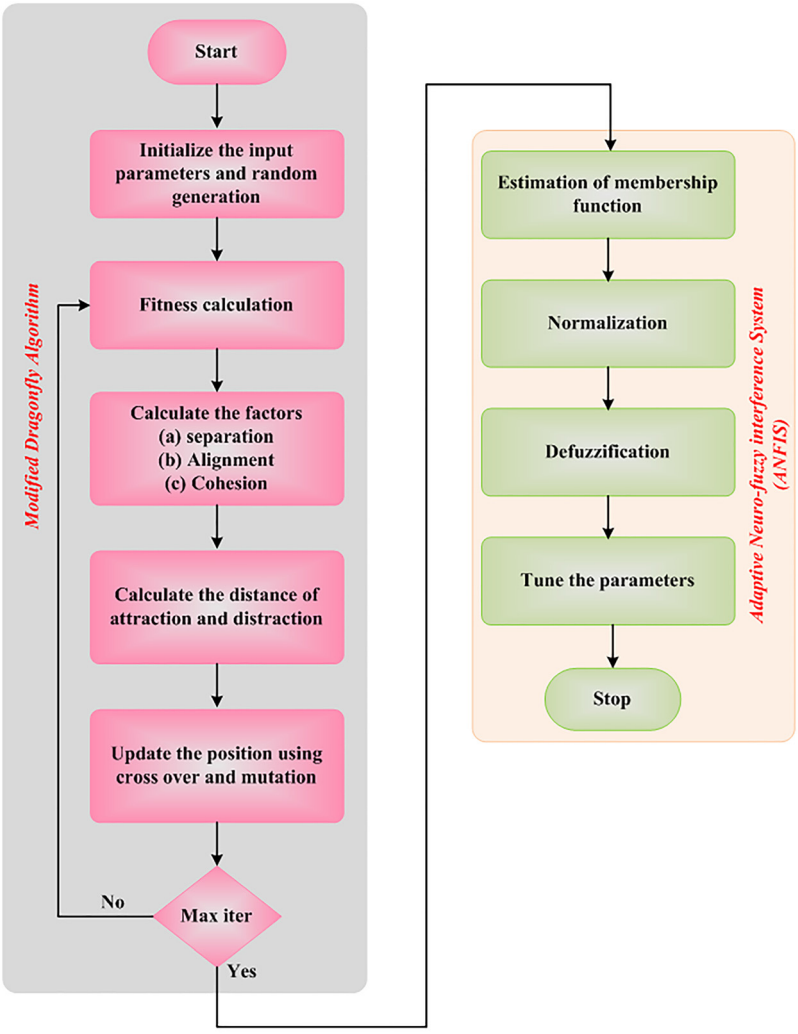

Fig. 3. Flowchart of proposed MDA-ANFIS approach

and W_{xy}^2 which is placed under the certain time interval and increased in the ANFIS.

2nd Layer: This layer shows the minimum error value based on the weights determined which is described as,

$$W_i = Min\left\{\left(W_{yz}^3(\Delta e), W_y^2(T_1), W_{xy}^2(T_2)\right)\right\} \tag{30}$$

$$\Delta e = e(t) - e(t-1) \tag{31}$$

here moment state error value is represented as $e(t)$, past condition of error is represented as $e(t-1)$, time intervals are represented as T_1, T_2.

The training values are input and output nodes and the expected values are obtained in the hidden layers, which has provides best output of the system.

3rd Layer: The value of weighted standardization process is determined by the following equation.

$$\overline{W}_i = \frac{W_i}{\sum W_i} \tag{32}$$

4th Layer: In this layer an adaptive node for de-fuzzification is calculated and the output is calculated below,

$$\overline{W}_k = \varepsilon_i x + \lambda_i y + (-\chi_i z) + r_i \tag{33}$$

Equation for the fourth layer output could be specified as,

$$Y_4 = \overline{W}_i f_i = \overline{W}_i(\varepsilon_i x + \lambda_i y + (-\chi_i z) + r_i \tag{34}$$

Here, $(\varepsilon = \lambda = \chi = 0)$, so the layer 4 output is described by,

$$Y_4 = \overline{W}_i f_i = \overline{W}_i(r_i) \tag{35}$$

5th Layer: This layer shows the weighted output of the parameter's resulting the summation value is given below,

$$Y_5 = \sum_i \overline{W}_i f = \frac{\sum_i \overline{W}_i f}{\sum_i \overline{W}_i} \tag{36}$$

At last, subsequent finishing of the algorithm, the ANFIS creates the optimal control signal.

6. RESULT AND DISCUSSIONS

This section describes the efficacy of the proposed method by simulation results. The proposed MDA-ANFIS approach is used to obtain the load power requirement in the hybrid wind photovoltaic system by 9-level inverter. The proposed approach is done in MATLAB/Simulink. The efficacy of the system is compared with the existing methods. Maximum power of hybrid wind solar system is obtained from the proposed method. The proposed method performance is analyzed under two cases, such as change of PV voltage and the change of wind voltage. The parameters of the proposed system are given in reference [35, 36].

Case 1: Change of PV Irradiation

In this case, the change of irradiance of PV based analysis is described. Figure 4 shows the analysis of PV irradiance temperature, the wind speed. In Fig. 4(a), the reference irradiance of the PV system is depicted. The irradiance is 1000 W m^{-2} at 0–0.5 sec. Then at 0.6–1 s, the irradiance is decreased to reach 400W m^{-2}. Figure 4(b) depicts the temperature of the system. It is constant to 25 °C at whole time. The speed of the wind is shown in Fig. 4(c). The speed of the whole system is 12 m s^{-1}. Figure 5 shows the analysis of voltage, current, power of PV and wind, PMSG speed torque, angle. The voltage of PV is shown in Fig. 5(a). The voltage of the system starts at 0.1 s then suddenly increases to reach 75 V. From 0.1 to 0.5 s time duration, the voltage value is around 75 V. At 0.5 s, the voltage value is decreased from 75 to 30 V. From 0.6 to 1 s the voltage value is 30 V.

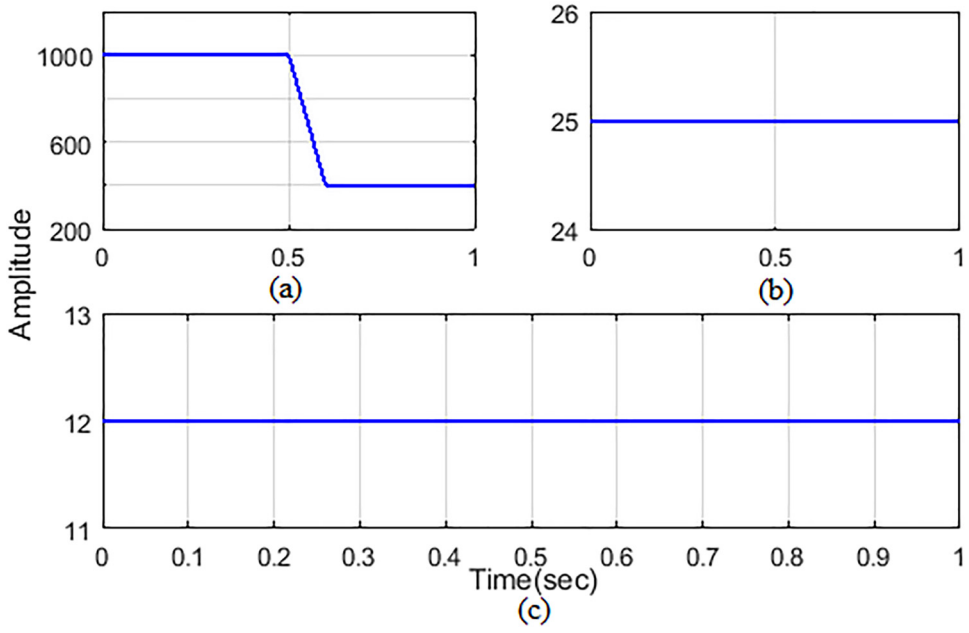

Fig. 4. Analysis of (a) PV irradiance (b) Temperature (c) Wind speed

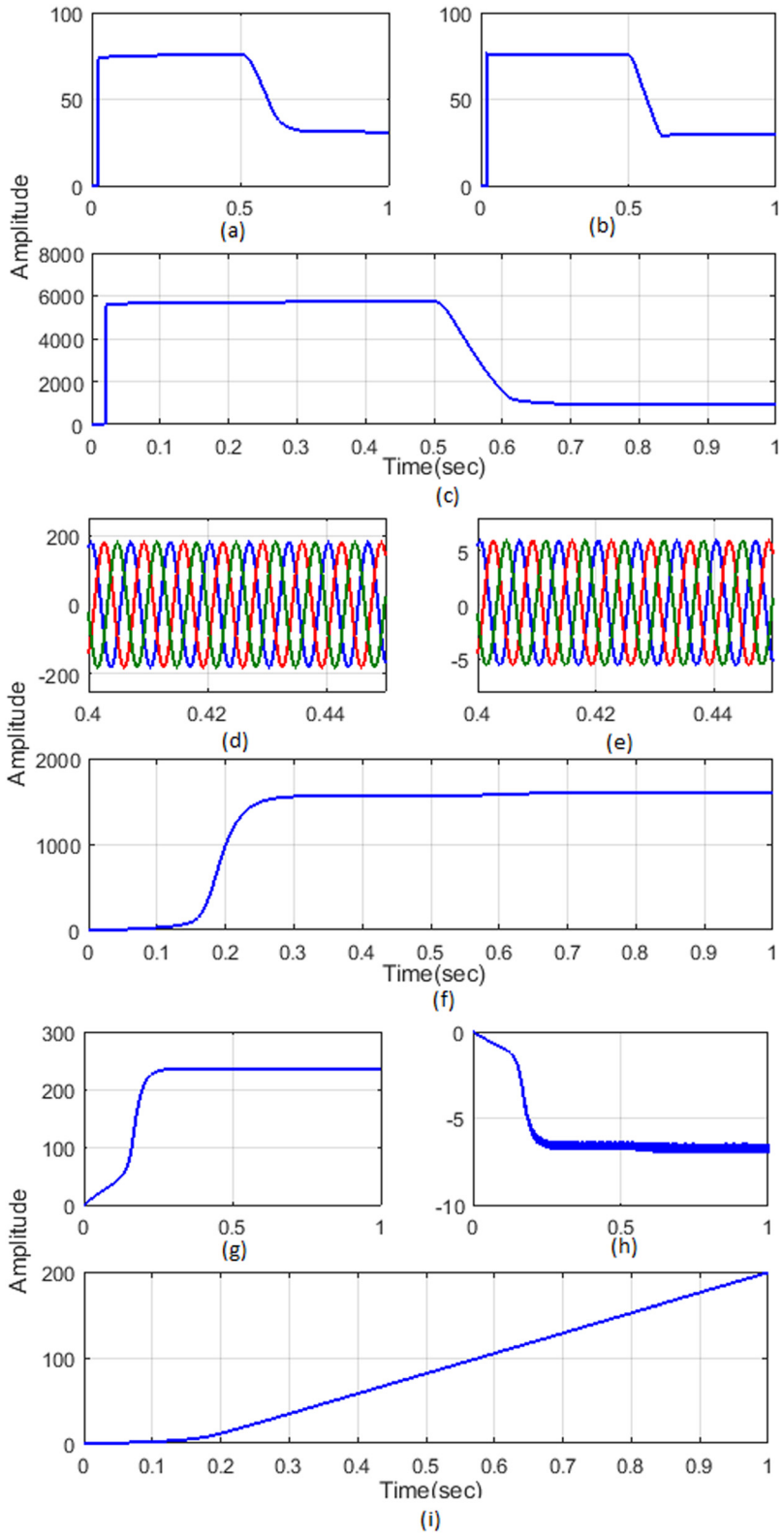

Fig. 5. Analysis of (a) PV voltage (b) PV current (c) PV power (d) Wind voltage (e) Wind current (f) Wind power (g) PMSG speed (h) PMSG torque (i) PMSG angle

Figure 5(b) represents the current analysis of PV system. At 0.6–1 s, the current also varied from 70 A at 0–0.5 s then it decreased to reach 30 A. Figure 5(c) shows the power analysis of PV system. The power of the PV starts at 0.01 s then suddenly to reaches 5900 W. From 0.01 to 0.5 s the power value is constant at 5900 W. Then the power value is decreased to reach 1000 W from 0.6 to 1 s. Figure 5(d) represents the wind voltage analysis. The wind voltage varies −200 V to +200 V. Figure 5(e) displays the analysis of wind current. The current is oscillated between the −5–5 A at 0.4–0.44 s. The wind power analysis is presented in Fig. 5(f). The wind power is changed from 0.05 s. From 0.1 s onwards it gradually increased to reach 1600 W. From 0.25 to 1 s the power value is 1600 W. Figure 5(g) represents the analysis of PMSG speed. The speed of PMSG is varied from 0 to 220 m s^{-1} at 0–0.3 s time duration. From 0.3 to 1 s the speed is constant to 220 m s^{-1}. The torque analysis of PMSG is shown in Fig. 5(h). The torque is varied from 0 to −7 at 0–0.3 s. From 0.3 to 1 s the torque value is constant to −7. From 0 to 200 at 0.05–1 s time, the PMSG angle is slightly increased.

Figure 6(a) displays the grid voltage of hybrid PV wind system. Here, the grid voltage varies from −1000 to 1000 V. At the same time, the current analysis is shown in Fig. 6(b). The current of grid is oscillating from −2 to 2 A. The grid power is shown in Fig. 6(c). The power starts at 0.03 s, and gradually increases to above 2000 W. From 0.03 to 1 s it is constant at above 2000 W. Figure 6(d) displays the analysis of load voltage and it oscillates from −1,000 to 1000 V from 0.4 to 0.46 s. The load current estimation is shown in Fig. 6(e). Here, the current varies from −9 to 9 A. The load power analysis is shown in Fig. 6(f). From 0 to 9000 W at 0–0.04 s the load power is increased. Then it is constant at 9000 W at 0.03–1 s. Figure 7 displays the inverter voltage system and varies from −200 to 200 V. Figure 8 displays the individual power analysis of the proposed, existing approaches. Figure 8(a) displays the individual power at normal condition. The power of load is increased from 0 to 9200 W at 0.02 s. From 0.3 to 1 s, the power is constant at 9200 W. The wind power starts at 0 and it raises from 0 to 1800 W at the time of 0.15–0.23 s. The wind power is constant at 1800 W at 0.23–1 s. The PV power starts at 0 then it

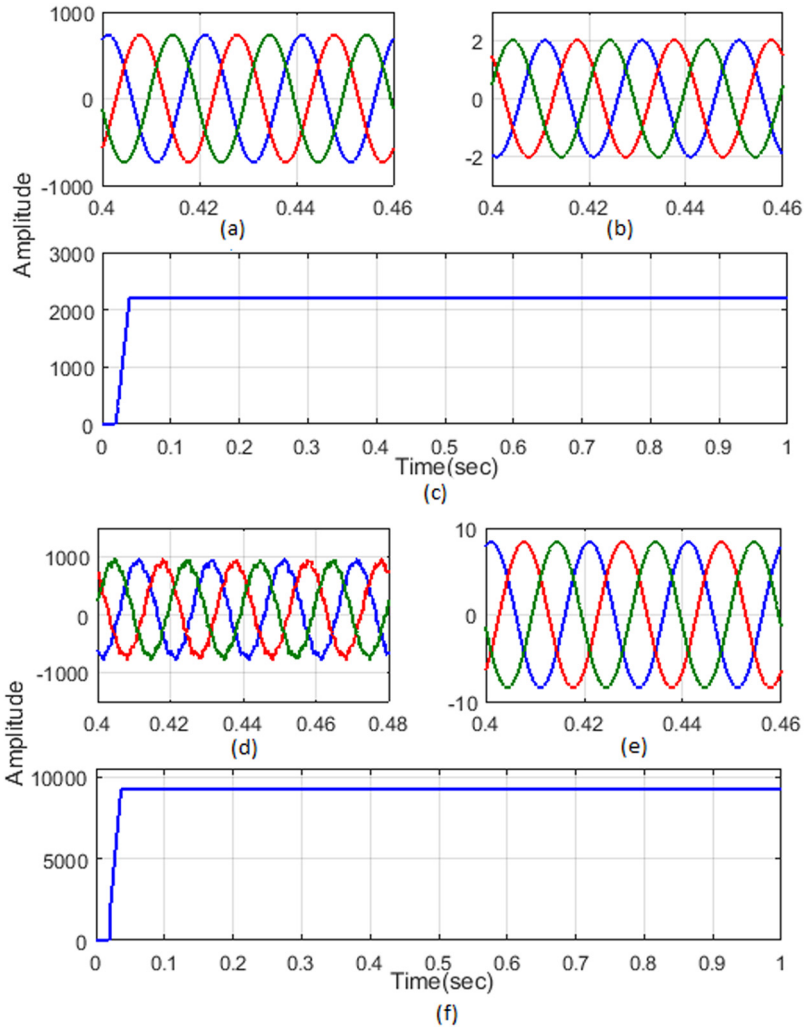

Fig. 6. Analysis of (a) Grid voltage (b) Grid current (c) Grid power (d) Load voltage (e) Load current (f) Load power

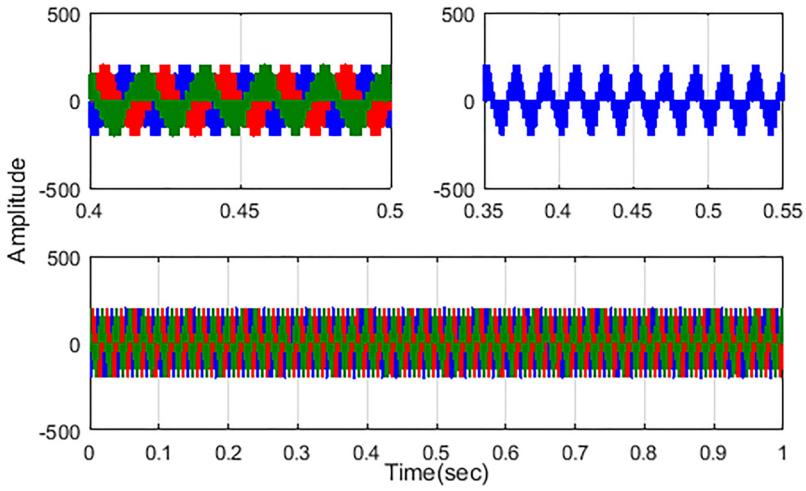

Fig. 7. Analysis of inverter voltage under the change of PV irradiance

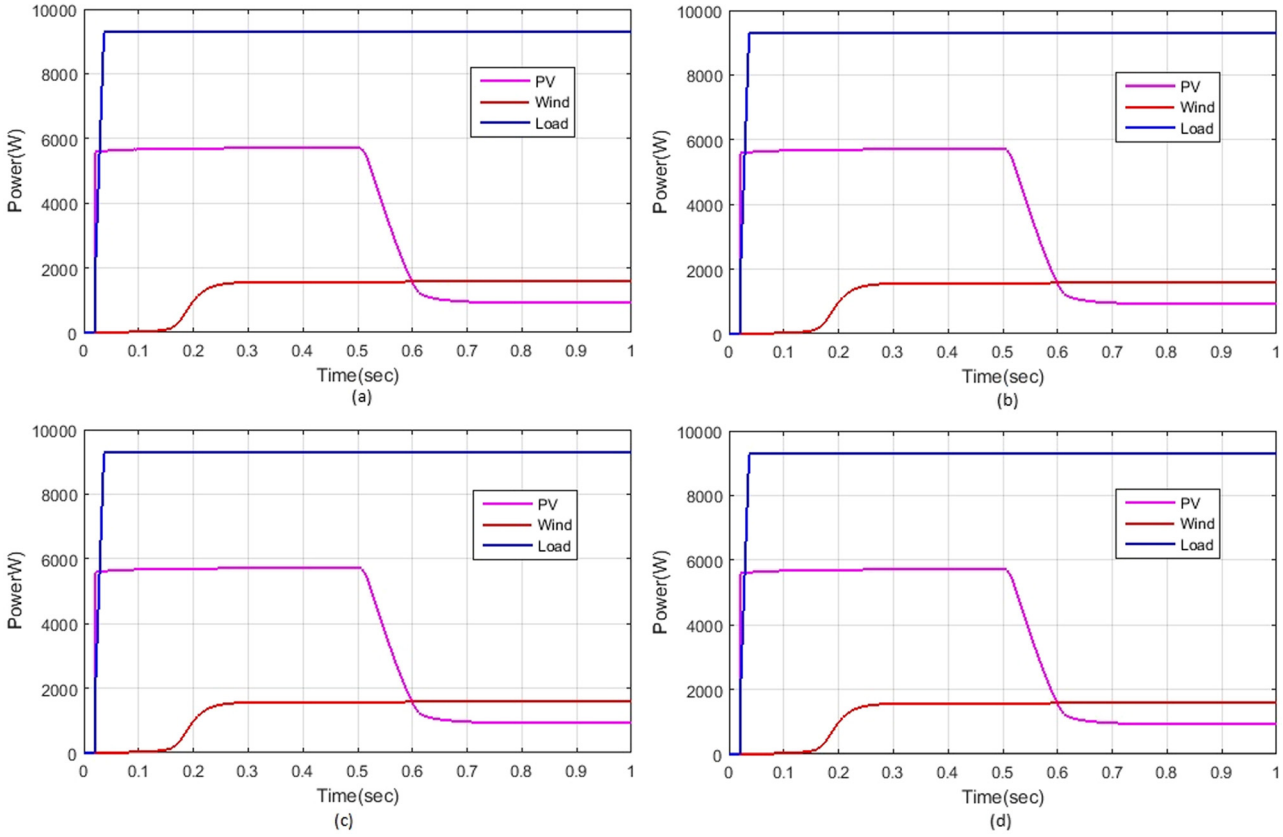

Fig. 8. Analysis of power in (a) Normal condition (b) Using MFO approach (c) Using MFORBFNN approach (d) Proposed system

raises to attain 5800 W at 0.01–0.5 s. At 0.5 s the power is lessened to attain 1000 W. The PV power is constant at 1000 W at 0.6–1 s. Figure 8(b) displays the individual power at the MFO approach. The power of load is increased from 0 to 9200 W at 0.02 s. From 0.3 to 1 s, the power is constant at 9200 W. At time 0.15–0.23 s, the wind power starts at 0 and it increases from 0 to 1800 W. The wind power is constant at 1800 W at 0.23–1 s. At 0.01–0.5 s, the PV power starts at 0 then it is maximized to attain 5800 W. At 0.5 s, the power is decreased to attain 1000 W. At 0.6–1 s, the PV power is constant at 1000 W. Figure 8(c) displays the individual power at the MFORBFNN approach. The power of load is increased from 0 to 9200 W at 0.02 s. From 0.3 to 1 s, the power is constant at 9200 W. At time 0.15–0.23 s, the wind power starts at 0 and it increases from 0 to 1800 W. The wind power is constant at 1800 W at 0.23–1 s. The PV

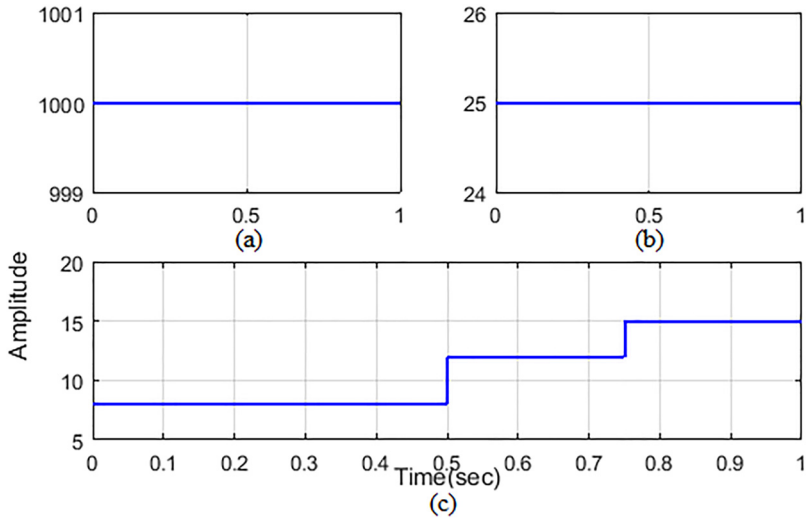

Fig. 9. Analysis of (a) PV irradiance (b) Temperature (c) Wind speed

power starts at 0 then it is maximized to attain 5800 W at 0.01–0.5 s. The power is lessened to 1000 W at 0.5 s. The PV power is constant at 1000 W at 0.6–1 s. Figure 8(d) displays the individual power at the proposed approach. The power of load is increased from 0 to 9200 W at 0.02 s. From 0.3 to 1 s, the power is constant to 9200 W. The wind power starts at 0 and it is increased from 0 to 1800 W at 0.15–0.23 s time. The wind power is constant at 1800 W at 0.23–1 s. The PV power starts at 0 then it is maximized to 5800 W at 0.01–0.5 s. To reach 1000 W, the power is reduced at 0.5 s. The PV power is constant at 1000 W at 0.6–1 s.

Case 2: Change of Wind Speed

Case 2 describes change of wind speed based analysis. Figure 9 shows the analysis of PV irradiance temperature, the wind speed. In PV system, reference irradiance is shown in Fig. 9(a). The irradiance is 1000 W m^{-2} at 0–1 s. i.e. it is constant at all times. The temperature of the system is shown in Fig. 9(b). It is constant to 25 °C the whole time. The speed of the wind is shown in Fig. 9(c). The speed of wind is 8 m s^{-1} at 0–0.5 s duration. Then the speed is raised to 12 m s^{-1} at 0.5–0.75 s. Then, at 0.75–1 s the speed is increased to reach 15 m s^{-1}. Figure 10 depicts the estimation of voltage, current, power of PV with wind, PMSG speed torque, angle. The voltage of PV is shown in Fig. 10(a). The voltage of the system is started at 0.1 s then suddenly increases to reach 75 V. From the time duration of 0.01–1 s the voltage value is around 75 V. Figure 10(b) illustrates the current analysis of PV system. Also at 0–1 s, the current is varied from 75 A. Figure 10(c) shows the power analysis of PV system. Powers of the PV is started at 0.01 s then suddenly reaches 5900 W. From 0.01 s to until the end of operation, the power value is constant at 5900 W. Figure 10 (d) shows the analysis of wind voltage. Initially wind voltage is varied around 0. Then it oscillates from −100 to 100 V. At the time duration of 0.5 s, the power value is slightly increased to reach −150 to 150 V. At 0.8 s again the wind voltage is increased from −200 V to +200 V. Figure 10(e) shows the analysis of wind current. Initially the current oscillates from 0 to 1 A at the time duration of 0–0.3 s. At 0.3 s–0.5 s, the current value is increased to reach −3 to 3 A. At 0.5 s again the current is increased to oscillate from −7 to 7 A. At 0.8 s, the current is increased to oscillate from −7–8 A. The wind power analysis is shown in Fig. 10(f). The wind power is changed from 0.05 s. From 0.25 s onwards it gradually increases to reach 800 W. From 0.5 s the power value is increased to reach 1500 W. It is constant at the period of 0.5–0.75 s. Then the power is again increased to reach 2500 W at 0.75–1 s time period. Figure 10(g) shows the analysis of PMSG speed. The speed of the PMSG is varied from 0 to 300 m s^{-1} at 0–1 s time duration. Initially the speed of the system starts at 0 to reach the value of 180 m s^{-1}. At 0.5 s, the speed is increased to reach 250 m s^{-1}. It is constant up to 0.8 s, then the speed is increased at 0.8 s time and at 0.3–1 s the speed is constant to 220 m s^{-1}. The torque analysis of PMSG is shown in Fig. 10(h). The torque is varied from 0 to −7 Nm at 0–0.3 s. From 0.3 to 1 s the torque value is constantly increased to reach −7 Nm. The angle increment of PMSG is shown in Fig. 10(i). The PMSG angle slowly increases from 0 to 180° angle at 0.25–1 s time. Figure 11(a) shows the analysis of grid voltage of hybrid PV wind system under wind speed change condition. The grid voltage is varied from −900 to 900 V. At the same time, the current analysis is shown in Fig. 11(b). The current of grid oscillates from −2 to 2 A. The grid power is shown in Fig. 11(c). The power starts at 0.03 s, and it slowly increases to reach above 2000 W. From 0.03 to 1 s it is constant at above 2000 W. Figure 11(d) shows the analysis of load voltage and it oscillates from −900 to 900 V from 0.8 to 1 s. The current analysis of load is shown in Fig. 11(e). The current is varied from −9 to 9 A. The load power analysis is shown in Fig. 11(f).

The load power increases from 0 to 9000 W at 0.01–1sec. Then at 0.01–1 s it is constant at 9000 W. The analysis of inverter voltage of the system under the change of wind speed is shown in Fig. 12. The inverter voltage is varied

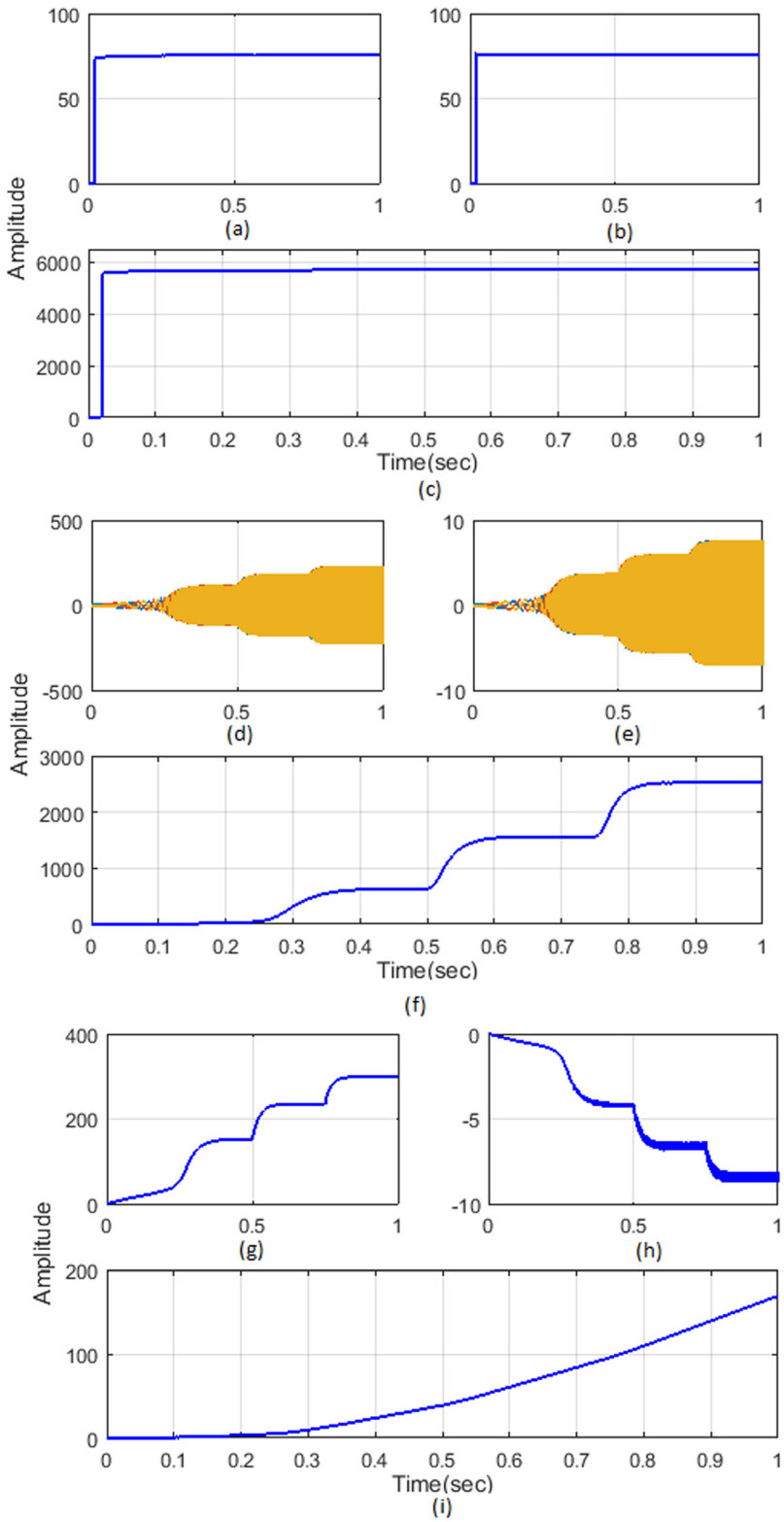

Fig. 10. Analysis of (a) PV voltage (b) PV current (c) PV power (d) Wind voltage (e) Wind current (f) Wind power (g) PMSG speed (h) PMSG torque (i) PMSG angle

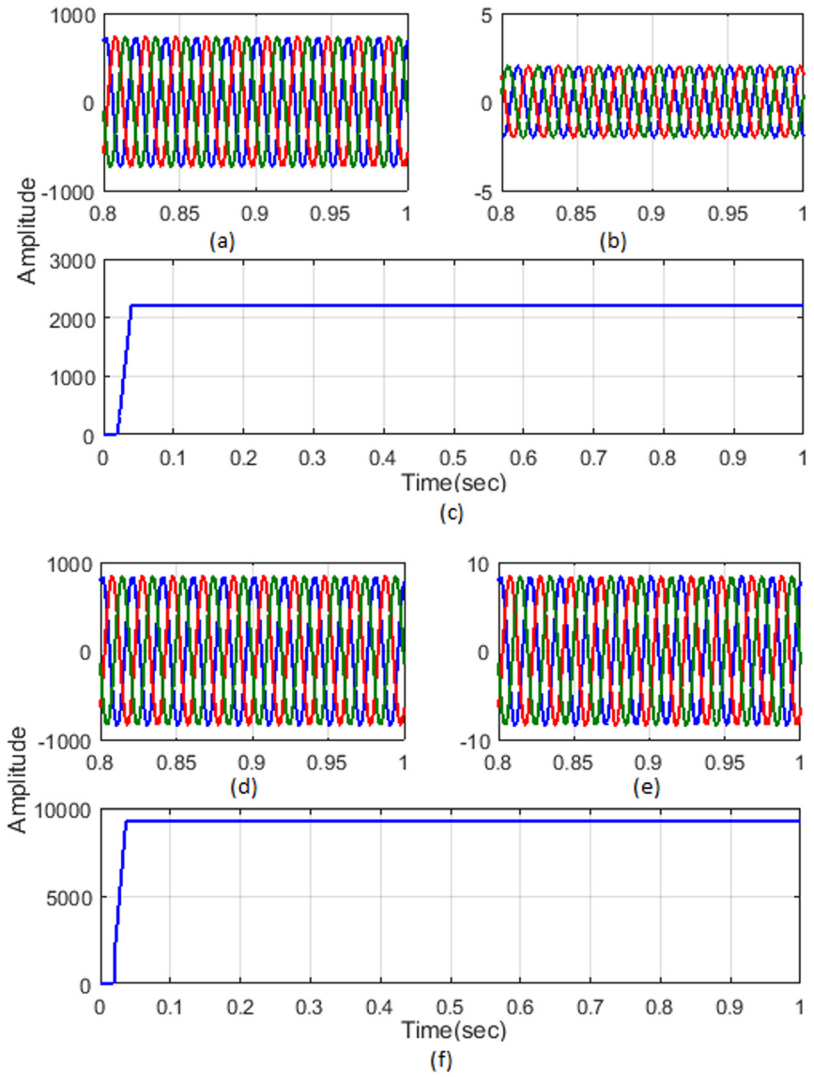

Fig. 11. Analysis of (a) Grid voltage (b) Grid current (c) Grid power (d) Load voltage (e) Load current (f) Load power under the wind speed change

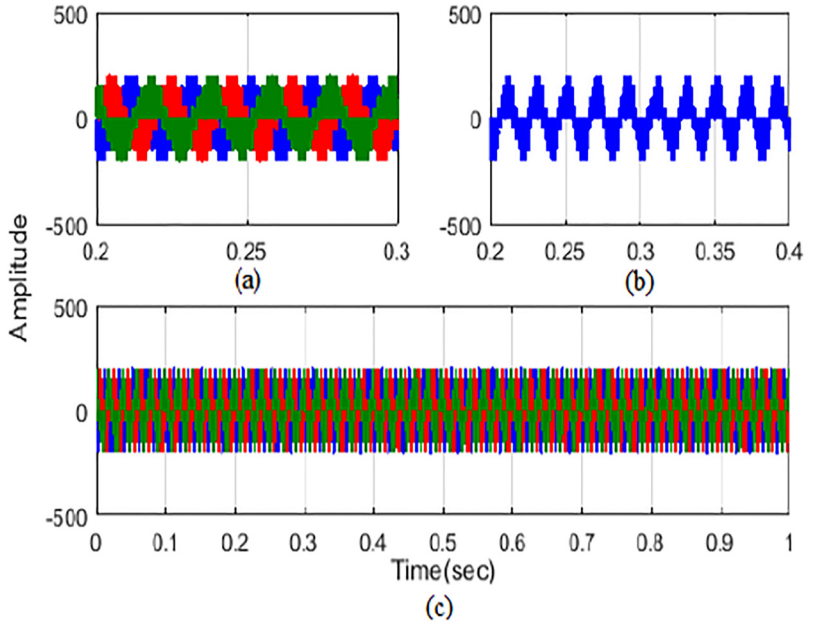

Fig. 12. Analysis of inverter voltage

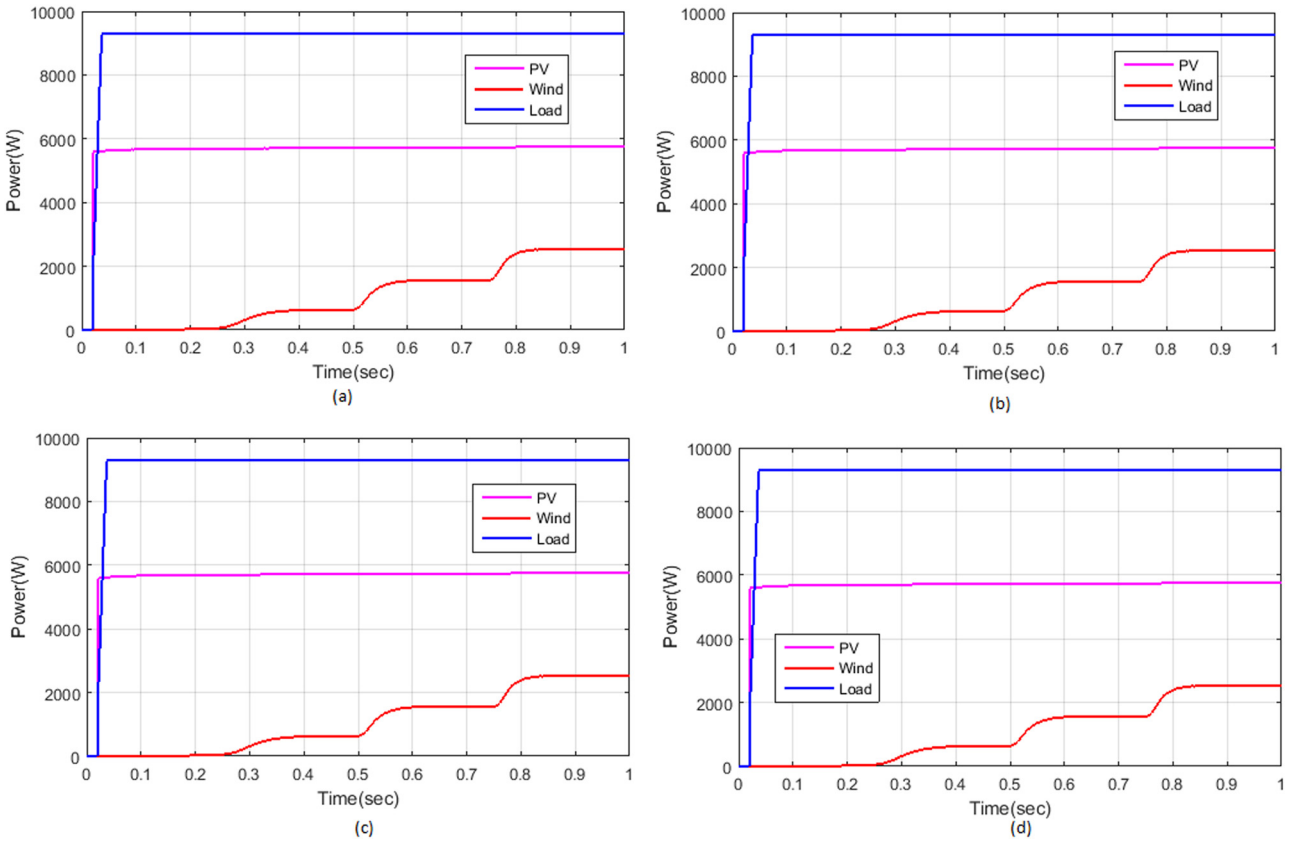

Fig. 13. Analysis of individual power in (a) Normal condition (b) using MFO approach (c) using MFORBFNN approach (d) Proposed system

from −200 to 200 V. Figure 13 shows the individual power analysis of the proposed, existing methods. Figure 8(a) demonstrates the individual power at normal condition. The power of load is increased from 0 to 9200 W at 0.02 s. From 0.3 to 1 s, the power is constant at 9200 W. The wind power starts at 0 and it increases from 0 to 2500 W at the time of 0.25–1 s. The wind power is increased from 0.25 s and reaches the value of 800 W until 0.5 s time period. At 0.5 s again the speed of the wind is increased to reach 1800 W at 0.75 s time period. At that point again the power is increased to reach 2500 W at 0.75–1 s. The PV power starts at 0 then it increases to reach 5800 W at 0.01–1 s. The individual power at the existing MFO approach is shown in Fig. 13(b). The power of load is increased from 0 to 9200 W at 0.02 s. From 0.3 to 1 s, the power is constant at 9200 W. The wind power starts at 0 and it increases from 0 to 2500 W at the time of 0.25–1 s. The wind power is increased from 0.25 s and reaches the value of 800 W until the time period of 0.5 s. At 0.5 s again the speed of the wind is increased to reach 1800 W at 0.75 s time period. At that point, again power is increased to reach 2500 W at 0.75–1 s time period. The PV power starts at 0 then it increases to reach 5800 W at 0.01–1 s. Figure 13(c) shows individual power at the MFORBFNN approach. The power of load is increased from 0 to 9200 W at 0.02 s. From 0.3 to 1 s, the power is constant at 9200 W. The wind power starts at 0 and it increases from 0 to 2500 W at 0.25–1 s time. The wind power increases from 0.25 s and reaches the value of 800 W until 0.5 s time period. At 0.5 s again the speed of the wind is increased to reach 1800 W at 0.75 s time period. At that point, again the power is increased to reach 2500 W at 0.75–1 s time period. The PV power starts at 0 then it increases to reach 5800 W at 0.01–1 s. Figure 13(d) shows an individual power of the proposed approach. The power of load is increased from 0 to 9200 W at 0.02 s. From 0.3 to 1 s, the power is constant at 9200 W. The wind power starts at 0 and it increases from 0 to 2500 W at 0.25–1 s time. The wind power is increased from 0.25 s and reaches the value of 800 W until 0.5 s time period. At 0.5 s, again the speed of the wind is increased to reach 1800 W at 0.75 s time period. Again the power is increased to reach 2500 W at 0.75–1 s time period. The PV power starts at 0 then it increases to reach 5800 W at 0.01–1 s.

Figure 14 shows the comparison of proposed and existing approaches through efficiency and THD. The analysis of efficiency in the proposed and existing method is shown in Fig. 14(a). The efficiency of the proposed system is high i.e. around 87% compared to the existing approaches like MDA-ANFIS, MFO. The Total harmonic distortion of the proposed and the existing method is shown in Fig. 14(b). The proposed approach THD is very low that is 1.6 compared to the existing approach. From this analysis, it is clearly visible that the proposed method provides optimal solution compared to the existing approaches.

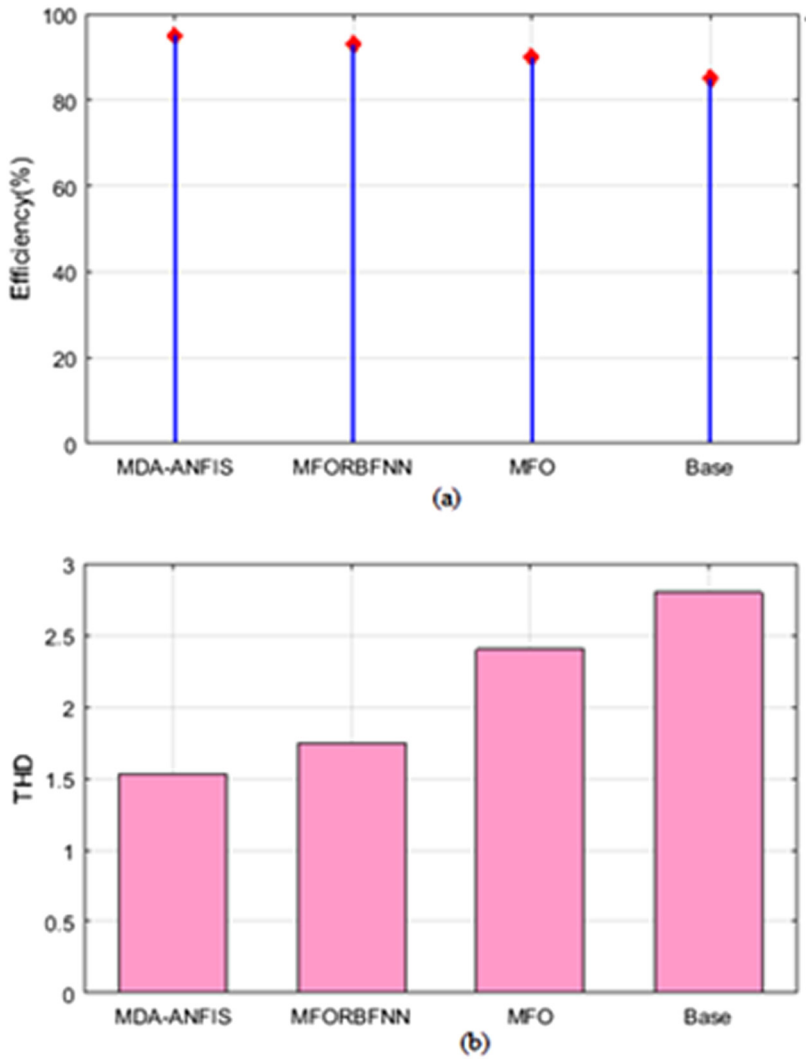

Fig. 14. Comparison of proposed and existing approaches through (a) Efficiency (b) THD analysis

7. CONCLUSION

This paper proposes an MDA-ANFIS approach with nine-level inverter to achieve the load requirement and to attain the high power of a hybrid wind solar system. The performance of the proposed technique is implemented in the MATLAB platform and compared with the existing approaches. The performance of the proposed hybrid technique is analyzed by comparing with existing techniques and also by using two different types of case studies such as change of PV voltage and the change of wind voltage. For all the cases, the proposed hybrid technique exhibits better performance in terms of grid power, load power, inverter voltage and so on. To prove the efficiency, the individual power of the proposed hybrid technique for all the cases is associated with MFO and MFO-RBFNN. From the simulation results, it is evident that the proposed hybrid technique possesses better output signal for the grid connected solar system with nine level inverter wind energy conversion.

Funding: This research did not receive any specific grant from funding agencies in the public, commercial, or not-for-profit sectors.

REFERENCES

[1] B. Sahoo, S. K. Routray, and P. K. Rout, "Repetitive control and cascaded multilevel inverter with integrated hybrid active filter capability for wind energy conversion system," *Eng. Sci. Technol. Int. J.*, vol. 22, no. 3, pp. 811–26, 2019.

[2] K. Janardhan, A. Mittal, and A. Ojha, "Performance investigation of stand-alone solar photovoltaic system with single phase micro multilevel inverter," *Energy Rep.*, vol. 6, pp. 2044–55, 2020.

[3] E. Barbie, R. Rabinovici, and A. Kuperman, "Analytical formulation and optimization of Weighted Total Harmonic Distortion in three-phase staircase modulated multilevel inverters," *Energy*, vol. 215, 2021, Paper no. 119137.

[4] M. Aly and H. A. Ramadan, "Design and implementation of adaptive SVPWM algorithm for multilevel inverters in

renewable energy applications," *Solar Energy*, vol. 183, pp. 745–54, 2019.

[5] B. G. Devi and B. K. Keshavan, "A novel hybrid phase shifted-modified synchronous optimal pulse width modulation based 27-level inverter for grid-connected PV system," *Energy*, vol. 178, pp. 309–17, 2019.

[6] R. Sepehrzad, M. E. Hassanzadeh, A. R. Seifi, and M. Mazinani, "An efficient multilevel interconnect control algorithm in AC/DC micro-grids using hybrid energy storage system," *Electric Power Syst. Res.*, vol. 191, p. 106869, 2021.

[7] F. H. Shajin, P. Rajesh, and S. Thilaha, "Bald eagle search optimization algorithm for cluster head selection with prolong lifetime in wireless sensor network," *J. Soft Comput. Eng. Appl.*, vol. 1, no. 1, p. 7, 2020.

[8] P. Rajesh, F. H. Shajin, and B. N. Kommula, "An efficient integration and control approach to increase the conversion efficiency of high-current low-voltage DC/DC converter," *Energy Syst.*, pp. 1–20, 2021.

[9] F. H. Shajin and P. Rajesh, "FPGA realization of a reversible data hiding scheme for 5G MIMO-OFDM system by chaotic key generation-based paillier cryptography along with LDPC and its side channel estimation using machine learning technique," *J. Circuits, Syst. Comput.*, vol. 31, no. 05, p. 2250093, 2022.

[10] P. Rajesh and F. H. Shajin, "Optimal allocation of EV charging spots and capacitors in distribution network improving voltage and power loss by Quantum-Behaved and Gaussian Mutational Dragonfly Algorithm (QGDA)," *Electric Power Syst. Res.*, vol. 194, p. 107049, 2021.

[11] M. Sandhu and T. Thakur, "Modified cascaded H-bridge multilevel inverter for hybrid renewable energy applications," *IETE J. Res.*, pp. 1–3, 2020.

[12] S. Gobimohan, "Active power quality improvement for unified renewable energy system with multilevel inverter and PEKF controllers," *Energy Sources A: Recovery, Util., Environ. Eff.*, vol. 42, no. 21, pp. 2603–22, 2020.

[13] P. R. Bana, K. P. Panda, S. Padmanaban, L. Mihet-Popa, G. Panda, and J. Wu, "Closed-loop control and performance evaluation of reduced part count multilevel inverter interfacing grid-connected PV system," *IEEE Access*, vol. 8, pp. 75691–701, 2020.

[14] A. Ramesh and H. H. Sait, "An approach towards selective harmonic elimination switching pattern of cascade switched capacitor twenty nine-level inverter using artificial bee colony algorithm," *Microprocess. Microsyst.*, vol. 79, p. 103292, 2020.

[15] A. Ul-Haq, M. Jalal, M. Aamir, C. Cecati, F. B. Muslim, A. A. Raja, and J. Iqbal, "Simulations and experimental validation of one cycle controlled nine-level inverter using FPGA," *Comput. Electr. Eng.*, vol. 88, p. 106885, 2020.

[16] O. Gulbudak and M. Gokdag, "Finite control set model predictive control approach of nine switch inverter-based drive systems: design, analysis, and validation," *ISA Trans.*, vol. 110, pp. 283–304, 2021.

[17] J. Liu, J. Wu, J. Zeng, and H. Guo, "A novel nine-level inverter employing one voltage source and reduced components as high-frequency AC power source," *IEEE Trans. Power Electron.*, vol. 32, no. 4, pp. 2939–47, 2016.

[18] K. Zare and M. Abapour, "Verification of a low component nine-level cascaded-transformer multilevel inverter in grid-tied mode," *IEEE J. Emerg. Sel. Top. Power Electron.*, vol. 6, no. 1, pp. 429–40, 2017.

[19] S. Pal, M. G. Majumder, R. Rakesh, K. Gopakumar, L. Umanand, D. Zielinski, and A. R. Beig, "A cascaded nine-level inverter topology with T-type and H-bridge with increased DC-bus utilization," *IEEE Trans. Power Electron.*, vol. 36, no. 1, pp. 285–94, 2020.

[20] J. C. Kartick, B. K. Sujit, and K. Suparna, "Dual reference phase shifted pulse width modulation technique for a N-level inverter based grid connected solar photovoltaic system," *IET Renew. Power Gen.*, vol. 10, no. 7, pp. 928–35, 2016.

[21] N. Sandeep and U.R. Yaragatti, "Operation and control of an improved hybrid nine-level inverter," *IEEE Trans. Ind. Appl.*, vol. 53, no. 6, pp. 5676–86, 2017.

[22] M. R. Singaravel, and S. A. Daniel, "MPPT with single DC–DC converter and inverter for grid-connected hybrid wind-driven PMSG–PV system," *IEEE Trans. Ind. Electron.*, vol. 62, no. 8, pp. 4849–57, 2015.

[23] F. Sebaaly, M. Sharifzadeh, H. Y. Kanaan, and K. Al-Haddad, "Multilevel switching-mode operation of finite-set model predictive control for grid-connected packed E-cell inverter," *IEEE Trans. Ind. Electron.*, vol. 68, no. 8, pp. 6992–7001, 2020.

[24] P. Kala and S. Arora, "Implementation of hybrid GSA SHE technique in hybrid nine-level inverter topology," *IEEE J. Emerg. Sel. Top. Power Electron.*, 2019.

[25] Y. Asano, Y. Ohno, S. Kurita, K. Kondo, T. Shinomiya, and K. Ishikawa, "Charge and discharge control to save regeneration energy for overhead line and energy storage device hybrid power source three-level inverter," *Electr. Eng. Jpn.*, vol. 202, no. 4, pp. 41–9, 2018.

[26] M. K. Das, K. C. Jana, and A. Sinha, "Performance evaluation of an asymmetrical reduced switched multi-level inverter for a grid-connected PV system," *IET Renew. Power Gen.*, vol. 12, no. 2, pp. 252–63, 2018.

[27] V. F. Pires, A. Cordeiro, D. Foito, and J. F. Silva, "Three-phase multilevel inverter for grid-connected distributed photovoltaic systems based in three three-phase two-level inverters," *Sol. Energy*, vol. 174, pp. 1026–34, 2018.

[28] T. V. Mahendiran, "A color harmony algorithm and extreme gradient boosting control topology to cascaded multilevel inverter for grid connected wind and photovoltaic generation subsystems," *Sol. Energy*, vol. 211, pp. 633–53, 2020.

[29] S. Saravanan, and T. S. Sivakumaran, "A hybrid technique used in grid integration of photovoltaic system for maximum power point tracking with multilevel inverter," *Trans. Inst. Meas. Control*, vol. 43, no. 1, pp. 215–27, 2021.

[30] B. Sharma, R. Dahiya, and J. Nakka, "Effective grid connected power injection scheme using multilevel inverter based hybrid wind solar energy conversion system," *Electric Power Syst. Res.*, vol. 171, pp. 1–4, 2019.

[31] A. I. Ali, M. A. Sayed, and T. Takeshita, "Isolated single-phase single-stage DC-AC cascaded transformer-based multilevel inverter for stand-alone and grid-tied applications," *Int. J. Electr. Power Energy Syst.*, vol. 125, p. 106534, 2021.

[32] B. Mahato, S. Majumdar, and K. C. Jana, "A new and generalized structure of single-phase and three-phase cascaded multilevel inverter with reduced power components," *Int. Trans. Electr. Energy Syst.*, vol. 30, no. 2, p. e12187, 2020.

[33] S. Mirjalili, "Dragonfly algorithm: a new meta-heuristic optimization technique for solving single-objective, discrete, and multi-

objective problems," *Neural Comput. Appl.*, vol. 27, no. 4, pp. 1053–73, 2016.

[34] R. N. Mishra, and K. B. Mohanty, "Real time implementation of an ANFIS-based induction motor drive via feedback linearization for performance enhancement," *Eng. Sci. Technol. Int. J.*, vol. 19, no. 4, pp. 1714–30, 2016.

[35] G. Chandra Sekhar, M. Venkatesh, and A. Appa Rao, "Wind energy source interfacing to grid byUsing five-level inverter," *J. C T A.*, vol. 10, no. 5, pp. 577–87, 2017.

[36] G. Chandra Sekhar, M. Rambabu, and A. Appa Rao, "Solar and wind energy sources interfacing to the utility grid using five level inverter," *Int. J. Eng. Technol. (Ijet)*, vol. 9, no. 2, 2017.